

Robust Wireless Power Transfer Waveform Design Using Waveform-to-Energy Harvesting Model

Konstantinos Ntougias*, Taneli Riihonen†, and Ioannis Krikidis*

*Department of Electrical and Computer Engineering, University of Cyprus, Cyprus

†Faculty of Information Technology and Communication Sciences, Tampere University, Finland

E-mail: kntoug01@ucy.ac.cy, taneli.riihonen@tuni.fi, krikidis@ucy.ac.cy

Abstract—Wireless power transfer (WPT) has emerged as a promising technology for prolonging the battery life of energy-constrained devices. Waveform optimization enhances energy harvesting efficiency, but depends on the applied energy harvesting model. Conventional models capturing rectifier nonlinearities unveiled multisines’ superiority over continuous waves, but exhibit limitations in supported waveforms and rectifier structures. A recently proposed waveform-to-energy harvesting model addresses these limitations and showed that pulsed radio frequency (RF) signals outperform multisines under ideal conditions. However, practical deployments face channel uncertainty. This paper presents a robust optimization framework for WPT systems under a bounded channel estimation error model. We develop an efficient algorithm maximizing worst-case harvested energy and propose single- and multi-frequency pulsed RF designs that maintain performance despite channel uncertainty. Numerical results demonstrate significant gains of the proposed designs over benchmarks, especially under severe channel uncertainty.

Index Terms—Wireless power transfer, energy harvesting efficiency, channel estimation errors, waveform-to-energy harvesting model, waveform optimization.

I. INTRODUCTION

Far-field wireless power transfer (WPT) enables energy delivery from radio frequency (RF) sources to low-power devices [1], [2]. Nonetheless, path loss deteriorates performance, necessitating waveforms that maximize the harvested energy. Conventional waveform-to-power energy harvesting (EH) models [3], [4] revealed that rectifier nonlinearities significantly impact RF-EH efficiency [3], [5] and demonstrated multisine signals’ superiority over continuous waves [3], [5]. Under these models, designs exploiting frequency-selective channels [6], [7] or joint waveform-beamforming optimization [8] and robust schemes under partial [4] or no [9] channel state information (CSI) have been developed.

However, these EH models restrict optimization to multisines with fixed frequencies, neglect bandwidth constraints, limit receiver structures to single-diode rectifiers, and assume perfect impedance matching. A recently proposed waveform-to-EH model [10] addresses these limitations, demonstrating that pulsed RF signals outperform multisines in single-antenna WPT systems. Nevertheless, [10] considers perfect CSI, which is an unrealistic assumption [6].

This work has received funding from the European Research Council through Horizon 2020 Research and Innovation Programme under Grant 819819, from the European Commission through Horizon-JU-SNS under Grants 101139291 and 101192080, and from the Ulla Tuominen foundation.

This paper develops a comprehensive framework for robust waveform design under channel uncertainty using the waveform-to-EH model. We analyze imperfect CSI’s impact using a bounded error model and develop waveforms that dynamically adjust their parameters based on the severity of channel uncertainty to maximize the worst-case harvested energy. Numerical evaluations demonstrate our designs’ effectiveness compared to benchmarks.

II. IDEAL SINGLE-ANTENNA WPT SYSTEM

A. System Model

We consider a single-antenna WPT system where the complex baseband transmit signal $x(t)$ corresponds to RF signal $\hat{x}(t) = \sqrt{2}\Re\{x(t)e^{j2\pi f_c t}\}$ with center frequency f_c and power constraint $P_{RF}^{out} = \mathbb{E}\{|x(t)|^2\} \leq P_{Tx}$. The baseband received signal is $y(t) = h(t) * x(t)$, where $h(t)$ is the channel response (receiver noise is negligible for EH). The instantaneous envelope power is $p(t) = 2|y(t)|^2$, and the average received power is $P_{RF}^{in} = \mathbb{E}\{|y(t)|^2\}$. After rectification, harvested DC power is $P_{out}^{dc} = (V_{out}^{dc})^2 / R_L$, where V_{out}^{dc} is the output voltage across load R_L . Different waveforms apply to this general model:

- **Multisine:** $x(t) = \sum_{n=1}^N A_n \exp[j2\pi f_n t + j\phi_n]$, with amplitude A_n , frequency f_n , phase ϕ_n for the n -th tone, and transmit power $P_{RF}^{out} = \sum_{n=1}^N A_n^2$. The average received power is $P_{RF}^{in} = \sum_{n=1}^N A_n^2 |H_n|^2$, where H_n is the frequency response at f_n .
- **Pulsed RF:** $x(t) = A \exp[j2\pi f t + j\phi] \cdot r(t)$, where $r(t)$ is a rectangular pulse train with duty cycle μ , period T , and $A = \sqrt{P_{Tx}/\mu}$. The average received power is $P_{RF}^{in} = |H(f)|^2 \cdot P_{Tx}$, where $H(f)$ is the frequency response.

B. Waveform-to-Energy Harvesting Model

The waveform-to-EH model [10] relates harvested DC power to the distribution of instantaneous envelope power:

$$P_{out}^{dc} = \mathbb{E}\{\eta(P) \cdot P\} = \int_0^\infty \eta(p) \cdot p \cdot f_P(p) dp, \quad (1)$$

where $\eta(p)$ is receiver efficiency for input power p , and $f_P(p)$ is the probability density function of envelope power.

C. Optimal Waveform Design

Using a two-stage optimization approach, the authors in [10] showed that the optimal power distribution is bimodal:

$$f_P^*(p) = (1 - \mu^*) \cdot \delta(p) + \mu^* \cdot \delta\left(p - \frac{P_{RF}^{in}}{\mu^*}\right), \quad (2)$$

implying a pulsed RF signal, where $\delta(p)$ is the Dirac delta function and the optimal duty cycle is:

$$\mu^* = \begin{cases} \frac{P_{RF}^{in}}{\bar{p}}, & P_{RF}^{in} \leq \bar{p} \\ 1, & P_{RF}^{in} > \bar{p} \end{cases}, \quad (3)$$

with $\bar{p} = \arg \max_p \eta(p)$.

The optimal baseband frequency f^* is given by:

$$f^* = \arg \max_f |H(f)|^2 \quad (4a)$$

$$\text{s.t. } f \in \left[-\frac{W}{2} + \frac{SW_{\min}}{2}, \frac{W}{2} - \frac{SW_{\min}}{2}\right], \quad (4b)$$

with amplitude $A = \sqrt{P_{Tx}/\mu^*}$. The minimum instantaneous bandwidth SW_{\min} and pulse duration τ_{\min} are related by:

$$\alpha \geq \sum_{m=0}^{\infty} \frac{(-1)^m (2\pi\tau B)^{2m+1}}{\pi(2m+1)(2m+2)!}, \quad (5)$$

where $\alpha \in (0, 1)$ controls spectral leakage, τ is pulse duration, and B is instantaneous bandwidth.

III. WPT WITH IMPERFECT CSI

A. System Model

Under imperfect CSI, the transmitter accesses an estimate $\tilde{H}(f)$ of the true channel $H(f)$:

$$H(f) = \tilde{H}(f) + \Delta(f), \quad \forall f \in [f_L, f_U], \quad (6)$$

where $\Delta(f)$ is channel estimation error with bound $|\Delta(f)| \leq \varepsilon |\tilde{H}(f)|$, $\varepsilon \in [0, 1)$ quantifying estimation quality.

Under this model, true channel amplitude is bounded as:

$$(1 - \varepsilon) |\tilde{H}(f)| \leq |H(f)| \leq (1 + \varepsilon) |\tilde{H}(f)|, \quad (7)$$

with phase uncertainty approximated by:

$$|\angle H(f) - \angle \tilde{H}(f)| \lesssim \varepsilon \quad \text{for small } \varepsilon. \quad (8)$$

B. Analytical Study

1) *Worst-Case Analysis for Single-Tone Transmission:* For single-tone transmission, envelope power $p(t) = 2A_1^2 |H(f_1)|^2$ is constant. Minimum power occurs when $|H(f_1)| = (1 - \varepsilon) |\tilde{H}(f_1)|$, resulting in $p_{\min} = 2A_1^2 (1 - \varepsilon)^2 |\tilde{H}(f_1)|^2$. Worst-case harvested power is:

$$P_{out, \min}^{dc} = \eta(2A_1^2 (1 - \varepsilon)^2 |\tilde{H}(f_1)|^2) \cdot 2A_1^2 (1 - \varepsilon)^2 |\tilde{H}(f_1)|^2. \quad (9)$$

2) *Worst-Case Analysis for Pulsed RF Waveform:* For pulsed RF, envelope power fluctuates between 0 and $p_{\text{peak}} = 2A^2 |H(f^*)|^2$. Worst-case peak power gives $p_{\text{peak}, \min} = 2A^2 (1 - \varepsilon)^2 |\tilde{H}(f^*)|^2$ and harvested power:

$$P_{out, \min}^{dc} = \mu^* \cdot \eta(2A^2 (1 - \varepsilon)^2 |\tilde{H}(f^*)|^2) \cdot 2A^2 (1 - \varepsilon)^2 |\tilde{H}(f^*)|^2. \quad (10)$$

C. Problem Formulation

Given the impact of channel uncertainty on harvested energy, we formulate a two-stage robust optimization problem to maximize worst-case performance.

1) *Receiver-Side Optimization:* We determine power distribution maximizing worst-case harvested DC power:

$$\max_{f_P(p) \geq 0} \min_{H(f) \in \mathcal{H}(f)} \int_0^\infty \eta(p) \cdot p \cdot f_P(p) dp \quad (11a)$$

$$\text{s.t. } \int_0^\infty p \cdot f_P(p) dp = P_{RF}^{in}, \quad (11b)$$

$$\int_0^\infty f_P(p) dp = 1, \quad (11c)$$

where $\mathcal{H}(f) = \{H(f) : H(f) = \tilde{H}(f) + \Delta(f), |\Delta(f)| \leq \varepsilon |\tilde{H}(f)|\}$ is the uncertainty set. The same formulation applies to multisine signals as well, by using the uncertainty set $\mathcal{H}_n = \{H_n : H_n = \tilde{H}_n + \Delta_n, |\Delta_n| \leq \varepsilon |\tilde{H}_n|, n = 1, 2, \dots, N\}$. Also, P_{RF}^{in} depends on the transmit waveform structure.

2) *Transmitter-Side Optimization:* We design a transmit waveform generating the optimal distribution while satisfying power and bandwidth constraints:

$$\max_{x(t)} \min_{H(f) \in \mathcal{H}(f)} P_{out}^{dc} \quad (12a)$$

$$\text{s.t. } \mathbb{E}\{|x(t)|^2\} = P_{Tx}, \quad (12b)$$

$$x(t) \text{ has bandwidth } \leq W. \quad (12c)$$

For multisine this problem becomes:

$$\max_{\{A_n, f_n, \phi_n\}} \min_{H(f_n) \in \mathcal{H}(f_n)} P_{out}^{dc} \quad (13a)$$

$$\text{s.t. } \sum_{n=1}^N A_n^2 = P_{Tx}, \quad (13b)$$

$$|f_n| \leq \frac{W}{2}, \quad \forall n \in [1, N], \quad (13c)$$

while for pulsed RF, we have:

$$\max_{A, f, \phi, \mu} \min_{H(f) \in \mathcal{H}(f)} P_{out}^{dc} \quad (14a)$$

$$\text{s.t. } A^2 \cdot \mu = P_{Tx}, \quad (14b)$$

$$|f| \leq \frac{W}{2} - \frac{SW_{\min}}{2}. \quad (14c)$$

D. Robust Waveform Design

1) *Optimal Power Distribution:* The worst-case harvested DC power occurs when the channel gains are at their lower bounds, resulting in $P_{RF, \min}^{in} = (1 - \varepsilon)^2 P_{RF}^{in}$. The optimal power distribution follows:

$$f_P^*(p) = (1 - \mu^*) \cdot \delta(p) + \mu^* \cdot \delta\left(p - \frac{(1 - \varepsilon)^2 P_{RF}^{in}}{\mu^*}\right), \quad (15)$$

with optimal duty cycle $\mu^* = \min((1 - \varepsilon)^2 P_{RF}^{in} / \bar{p}, 1)$.

2) *Optimal Waveform Structure*: Under channel uncertainty, frequency diversity becomes beneficial. We propose:

- **Robust Single-Frequency (SF) Pulsed RF**: maintains pulsed structure, but selects the frequency maximizing the worst-case harvested power.
- **Multi-Frequency (MF) Pulsed RF**: transmits multiple pulses simultaneously at different frequencies with optimized power allocation.

3) *Robust SF Pulsed RF Design*: The optimal signal is:

$$x^*(t) = A_{\text{robust}} \exp[j2\pi f_{\text{robust}}^* t + j\phi^*] \cdot r(t), \quad (16)$$

where $A_{\text{robust}} = \sqrt{P_{Tx}/\mu^*}$ and

$$f_{\text{robust}}^* = \arg \max_f \Gamma(f) \cdot (1 - \varepsilon)^2 |\tilde{H}(f)|^2 \quad \text{s.t. (6b)}. \quad (17)$$

Here, $\Gamma(f) = 1 - \beta \cdot \frac{\sigma_{|\tilde{H}|^2}(f)}{\mu_{|\tilde{H}|^2}(f)}$ is a stability factor quantifying channel reliability at frequency f with $\beta \in [0, 1]$ controlling the impact of channel variability on frequency selection and $\sigma_{|\tilde{H}|^2}(f)$ and $\mu_{|\tilde{H}|^2}(f)$ representing the standard deviation and mean, respectively, of channel gains in the vicinity of f .

4) *Multi-Frequency (MF) Pulsed RF Design*: The signal is $x^*(t) = \sum_{k=1}^K A_k \exp[j2\pi f_k^* t + j\phi_k^*] \cdot r(t)$, where the number of tones K adapts to channel uncertainty:

$$K = \min \left(\left\lceil \frac{1}{1 - \varepsilon} \right\rceil, K_{\max} \right). \quad (18)$$

The frequencies are selected by:

$$\{f_1^*, f_2^*, \dots, f_K^*\} = \arg \max_{\{f_1, \dots, f_K\}} \min_{1 \leq k \leq K} (1 - \varepsilon)^2 |\tilde{H}(f_k)|^2 \quad (19a)$$

$$\text{s.t. } |f_k| \leq \frac{W}{2}, \quad \forall k \in [1, K], \quad (19b)$$

$$|f_i - f_j| \geq \frac{SW_{\min}}{2}, \quad \forall i \neq j, \quad (19c)$$

where (19b) restricts frequencies within the bandwidth and (19c) restricts tone separation to ensure spectral containment.

With optimal phases for maximum constructive combining $\phi_k = -\angle \tilde{H}(f_k)$, peak envelope power becomes:

$$p_{\text{peak}} = \frac{2(1 - \varepsilon)^2 \left(\sum_{k=1}^K A_k |\tilde{H}(f_k)| \right)^2}{\mu^*}, \quad (20)$$

yielding harvested power $P_{\text{out}}^{dc} = \mu^* \cdot \eta(p_{\text{peak}}) \cdot p_{\text{peak}}$.

For the low-power regime where $\mu^* < 1$, the power allocation problem can be formulated as

$$\max_{\{A_k\}_{k=1}^K} \frac{(1 - \varepsilon)^2 \sum_{k=1}^K A_k^2 |\tilde{H}(f_k)|^2}{\bar{p}} \cdot \eta(p_{\text{peak}}) \cdot p_{\text{peak}} \quad \text{s.t. (19b)} \quad (21)$$

with $p_{\text{peak}} = \frac{2\bar{p}(\sum_{k=1}^K A_k |\tilde{H}(f_k)|)^2}{(1 - \varepsilon)^2 \sum_{k=1}^K A_k^2 |\tilde{H}(f_k)|^2}$. This non-convex problem can be solved efficiently using sequential convex programming (SCP) with projected gradient ascent (PGA), as shown in Algorithm 1 and Algorithm 2, respectively. SCP computes

the gradient $\mathbf{g} = [g_1, \dots, g_K]^T$ and Hessian matrix \mathbf{H} of the objective function $J = \mu^* \cdot \eta(p_{\text{peak}}) \cdot p_{\text{peak}}$ with respect to the amplitude variables, i.e., $g_i = \partial J / \partial A_i$ and $H_{i,j} = \partial^2 J / \partial A_i \partial A_j$, $i, j = 1, \dots, K$ (see Appendix A). Then, it computes the second-order Taylor series approximation of the objective function around the current point $\mathbf{A}^{(t)}$:

$$\hat{J}(\mathbf{A}) = J^{(t)} + (\mathbf{A} - \mathbf{A}^{(t)})^T \mathbf{g}^{(t)} + \frac{1}{2} (\mathbf{A} - \mathbf{A}^{(t)})^T \mathbf{H}^{(t)} (\mathbf{A} - \mathbf{A}^{(t)}), \quad (22)$$

where $\mathbf{A} = [A_1, A_2, \dots, A_K]^T$, to transform the original problem into a sequence of convex subproblems:

$$\max_{\mathbf{A}} \hat{J}(\mathbf{A}) \quad \text{s.t.} \quad \sum_{k=1}^K A_k^2 = P_{Tx}. \quad (23)$$

The PGA method with backtracking line search tackles these subproblems. PGA iteratively updates the power allocation through a gradient step followed by a projection onto the feasible set. Let $\mathbf{A}^{(t,l)}$ denote the power allocation at the l -th inner iteration within the t -th SCP iteration, with $\mathbf{A}^{(t,0)} = \mathbf{A}^{(t)}$. The update rule is

$$\mathbf{v} = \mathbf{A}^{(t,l)} + \varpi_l \nabla \hat{J}(\mathbf{A}^{(t,l)}), \quad (24a)$$

$$\mathbf{A}^{(t,l+1)} = \mathcal{P}_{\mathcal{S}}(\mathbf{v}) = \sqrt{P_{Tx}} \cdot \frac{\mathbf{v}}{\|\mathbf{v}\|_2}, \quad (24b)$$

where $\varpi_l > 0$ is the adaptive step size which is determined by Armijo rule, $\nabla \hat{J}(\mathbf{A}^{(t,l)}) = \mathbf{g}^{(t)} + \mathbf{H}^{(t)}(\mathbf{A}^{(t,l)} - \mathbf{A}^{(t)})$ is the gradient of the approximated objective, and $\mathcal{P}_{\mathcal{S}}(\cdot)$ is the projection operator onto the feasible set $\mathcal{S} = \{\mathbf{A} \in \mathbb{R}^K : \sum_{k=1}^K A_k^2 = P_{Tx}\}$. Upon convergence of the inner iterations, we set $\mathbf{A}^{(t+1)} = \mathbf{A}^{(t,l+1)}$ and proceed to the next outer (i.e., SCP) iteration. The SCP algorithm preferentially allocates power to frequencies with stronger channel gains while accounting for uncertainty.

We emphasize that the quadratic surrogate \hat{J} in (22) obtained by second-order Taylor expansion is not, in general, a global lower bound of the true objective J . Instead of relying on a global minorization property, we enforce a standard Armijo backtracking rule applied to the *true* objective J in each PGA update. Specifically, a candidate point $\mathbf{A}^{(t,l+1)}$ is accepted only if it yields a sufficient increase in J relative to $\mathbf{A}^{(t,l)}$; otherwise, the step size ϖ_l is reduced until the Armijo condition is satisfied. This safeguard ensures that the sequence $\{J(\mathbf{A}^{(t)})\}$ is non-decreasing. Since the feasible set \mathcal{S} is compact and J is continuously differentiable, all iterates remain bounded [11], and every accumulation point of the SCP procedure is a stationary point of the original problem.

5) *Minimum Pulse Duration Constraint*: The minimum pulse duration τ_{\min} (found by solving (5)) constrains duty cycle $\mu \geq \mu_{\min} = \frac{\tau_{\min}}{T}$, resulting in:

$$\mu_{\text{constrained}}^* = \max(\mu^*, \tau_{\min}/T). \quad (25)$$

Algorithm 1 SCP for MF Pulsed RF Power Allocation

Require: $\{|\tilde{H}(f_k)|\}_{k=1}^K, \varepsilon, P_{Tx}, \eta(p), \xi_{thr}, t_{max}$
1: Initialize: $t = 0, \xi^{(0)} = \infty, A_k^{(0)} = \sqrt{P_{Tx}/K} \forall k$
2: $\bar{p} = \arg \max_p \eta(p)$
3: **while** $\xi^{(t)} > \xi_{thr}$ and $t < t_{max}$ **do**
4: $P_{RF,min}^{in,(t)} = (1 - \varepsilon)^2 P_{RF}^{in,(t)}$
5: $\mu^{*,(t)} = \min((1 - \varepsilon)^2 P_{RF}^{in,(t)} / \bar{p}, 1)$
6: Calculate $p_{peak}^{(t)}$ using (20)
7: $J^{(t)} = \mu^{*,(t)} \cdot \eta(p_{peak}^{(t)}) \cdot p_{peak}^{(t)}$
8: Compute gradient $\mathbf{g}^{(t)}$ and Hessian $\mathbf{H}^{(t)}$
9: Update $\mathbf{A}^{(t+1)}$ using Algorithm 2
10: $\xi^{(t+1)} = \frac{\|\mathbf{A}^{(t+1)} - \mathbf{A}^{(t)}\|_2}{\|\mathbf{A}^{(t)}\|_2}, t \leftarrow t + 1$
11: **end while**
12: **return** $\{A_k^*\} = \{A_k^{(t)}\}$

Algorithm 2 Projected Gradient Ascent with Armijo Safeguard

Require: $\mathbf{A}^{(t)}, \mathbf{g}^{(t)}, \mathbf{H}^{(t)}, P_{Tx}, \xi_{inner}, L_{max}$
1: Initialize $l = 0, \mathbf{A}^{(t,0)} = \mathbf{A}^{(t)}, \xi = \infty$
2: **while** $\xi > \xi_{inner}$ and $l < L_{max}$ **do**
3: $\nabla J(\mathbf{A}^{(t,l)}) = \mathbf{g}^{(t)} + \mathbf{H}^{(t)}(\mathbf{A}^{(t,l)} - \mathbf{A}^{(t)})$
4: Compute step size ϖ_l by Armijo backtracking on *true* objective J
5: $\mathbf{v} = \mathbf{A}^{(t,l)} + \varpi_l \nabla J(\mathbf{A}^{(t,l)})$
6: $\mathbf{A}^{(t,l+1)} = \sqrt{P_{Tx}} \cdot \frac{\mathbf{v}}{\|\mathbf{v}\|_2}$
7: $\xi = \frac{\|\mathbf{A}^{(t,l+1)} - \mathbf{A}^{(t,l)}\|_2}{\|\mathbf{A}^{(t,l)}\|_2}, l = l + 1$
8: **end while**
9: **return** $\mathbf{A}^{(t+1)} = \mathbf{A}^{(t,l)}$

6) *Robust Waveform Design Algorithm:* We propose Algorithm 3 for robust waveform design in WPT systems with imperfect CSI. This algorithm enables flexible selection between transmission strategies depending on system requirements and channel conditions. Owing to the intrinsic non-convexity of the underlying optimization, the algorithm guarantees only local optimality. In particular, the SCP procedure converges to stationary points that satisfy the Karush–Kuhn–Tucker (KKT) conditions. Also, the robust min–max formulation provides a built-in performance safeguard: it optimizes against the worst admissible channel realization, thereby yielding conservative guarantees on the harvested power.

Each inner iteration of the PGA algorithm requires $\mathcal{O}(K^2)$ operations for gradient computation involving matrix-vector multiplication. Similarly, computing the gradient and Hessian in SCP requires $\mathcal{O}(K^2)$ operations. Thus, the overall worst-case complexity of the SF and MF designs is $\mathcal{O}(|W|)$ and $\mathcal{O}(|W| \log K + t_{max} L_{max} K^2)$ due to phase alignment or/and frequency selection. Clearly, the SF design is suitable for real-time operation, while the MF design suits well scenarios with stricter robustness and more relaxed delay demands.

IV. NUMERICAL EVALUATIONS

We evaluate the performance of our proposed robust designs against continuous wave (CW), optimized multisine, and non-robust pulsed RF waveforms through numerical simulations of a single-antenna WPT system with nonlinear rectifier under frequency-selective fading. The rectifier efficiency function $\eta(p)$ is derived from measured data [10], with maximum efficiency at $\bar{p} = 15$ dBm. We consider a channel with 6

Algorithm 3 Robust Waveform Design with Imperfect CSI

Require: $\tilde{H}(f), \varepsilon, P_{Tx}, W, \eta(p)$
1: Calculate $\bar{p} = \arg \max_p \eta(p)$ and $(1 - \varepsilon)^2 |\tilde{H}(f)|^2$
2: Select strategy based on channel characteristics and uncertainty level
3: Calculate channel stability factor $\Gamma(f)$ for frequency selection
4: Select optimal frequency(ies) using (17) or (19)
5: Calculate $\mu^* = \min((1 - \varepsilon)^2 P_{RF}^{in} / \bar{p}, 1)$
6: Set amplitude(s) and phase(s) based on selected strategy
7: Determine τ_{min} using (5)
8: **return** Waveform parameters

Rayleigh-distributed taps and exponential power decay (delay spread $\sigma_\tau = 100$ ns); $P_{Tx} = 30$ dBm; distance $d = 7$ m; path loss exponent $\alpha_{PL} = 3.5$; $W = 10$ MHz; $f_c = 868$ MHz; $\alpha = 0.9$; $T = 1$ μ s; and load resistance $R_L = 3.3$ k Ω . Results are averaged over 1000 channel realizations.

Rectifier's efficiency curve is shown in Fig. 1. The figure illustrates a nonlinear efficiency characteristic that peaks at approximately 51% when the input RF power reaches approximately 15 dBm. This bell-shaped efficiency profile is typical of rectifier circuits used in wireless power transfer systems, demonstrating the significant impact of input power levels on energy conversion effectiveness. Two distinct operational modes are highlighted in the figure. The continuous operation mode achieves approximately 23% efficiency at -10 dBm, while the pulsed operation mode (with 5% duty cycle) attains a higher efficiency of about 29% at -5 dBm. This comparison demonstrates a fundamental principle of the waveform-to-energy harvesting model: by concentrating available power into shorter pulses (i.e., reducing duty cycle), the system can operate at higher instantaneous power levels that correspond to more efficient regions of the rectifier's characteristic curve. The sharp decline in efficiency beyond 15 dBm emphasizes the importance of precise power control in WPT systems, as exceeding the optimal power point rapidly diminishes conversion efficiency. This nonlinear behavior directly validates our optimization approach, which aims to maximize harvested energy by operating as close as possible to the peak efficiency region under channel uncertainty constraints.

Fig. 2 illustrates the harvested DC power versus CSI error bound ε at $P_{Tx} = 30$ dBm. The results reveal several important trends. First, all designs show degradation as channel uncertainty increases, but with significantly different sensitivities to estimation errors. The robust multi-frequency (MF) pulsed RF design demonstrates exceptional performance, achieving approximately 310 μ W at $\varepsilon = 0.05$, which is substantially higher than all other approaches. This peak coincides with the transition from single to dual-frequency operation, optimally balancing diversity gain with combining challenges.

Notably, the robust MF design maintains superior performance across the entire uncertainty range, delivering approximately 150 μ W even at severe channel uncertainty ($\varepsilon = 0.5$)—about $3\times$ the power harvested by non-robust pulsed RF at the same uncertainty level. The robust single-frequency (SF) pulsed RF design also shows significant resilience to channel uncertainty, outperforming its non-robust counterpart

by approximately 30% at $\varepsilon = 0.3$ and 80% at $\varepsilon = 0.5$, indicating the quick degradation of non-robust schemes as the CSI uncertainty becomes severe. In contrast, multisine waveforms present inferior performance compared to the pulsed RF designs, with growing performance loss as the number of tones increases from 2 to 16, contradicting their theoretical superiority under perfect CSI. This degradation results from compounding estimation errors across multiple frequencies, increasing destructive interference probability and causing sub-optimal power allocation. In alignment with the above, CW design outperforms two-tones signal.

Fig. 3 depicts the relationship between duty cycle and channel uncertainty. We note that both robust designs have very small duty-cycle. This reflects the fact that the received power is far below $\bar{p} \approx 31.62$ mW, thus requiring short pulses for improved efficiency. We also note that that in both variants, the duty cycle peaks at $\varepsilon = 0.05$ and then remains constant, corresponding to slope change for the curve in Fig. 2.

Fig. 4 examines the impact of transmit power on harvested energy at $\varepsilon = 0.3$. The results reveal a clear power threshold around 15 dBm, below which negligible energy is harvested regardless of waveform design. This threshold behavior stems from the exponential relationship between distance and received power under path loss, combined with the efficiency characteristics of the energy harvesting circuit. As transmit power increases beyond 20 dBm, the performance gap between different waveform designs becomes more pronounced. The robust MF design demonstrates the highest harvested power across the entire high-power region, outperforming the non-robust pulsed RF by up to 85% at 30 dBm.

Fig. 5 provides valuable insight into the frequency selection behavior of both robust and non-robust SF designs under varying channel uncertainty. At $\varepsilon = 0$, both approaches select frequency indices with maximum channel gain. However, as ε increases to 0.2 and 0.5, the robust design increasingly favors frequencies with better stability characteristics, as quantified by the $\Gamma(f)$ factor. This adaptive frequency selection represents a key mechanism via which the robust design maintains performance under uncertainty, strategically trading nominal channel gain for reliability when estimation quality degrades.

These results demonstrate the substantial benefits of the proposed robust designs in WPT deployments with imperfect CSI. Adaptive frequency selection and power allocation mechanisms ensure consistent EH performance across diverse operating conditions and channel estimation qualities.

V. CONCLUSION

We presented the first robust optimization framework combining the novel waveform-to-EH model [10], which enables optimization over arbitrary waveform distributions and accounts for bandwidth limitations, with bounded channel uncertainty for WPT systems. To characterize the performance gains of robust versus non-robust designs, we employed the setup and assumptions of the baseline work [10]. According to numerical results, the proposed SF design, which is suitable for real-time operation, achieves 30-35% improvement

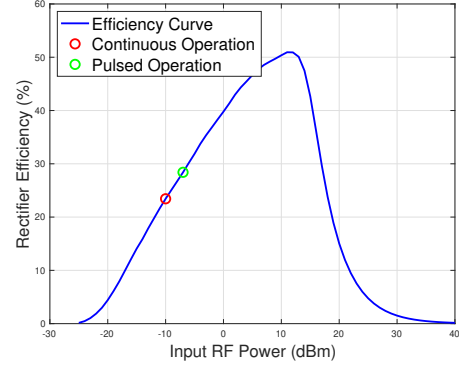


Fig. 1. Rectifier's efficiency.

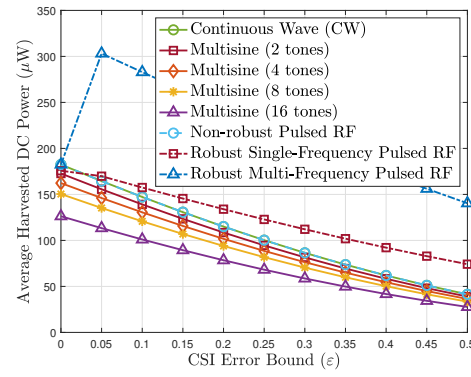


Fig. 2. Impact of channel uncertainty on harvested power.

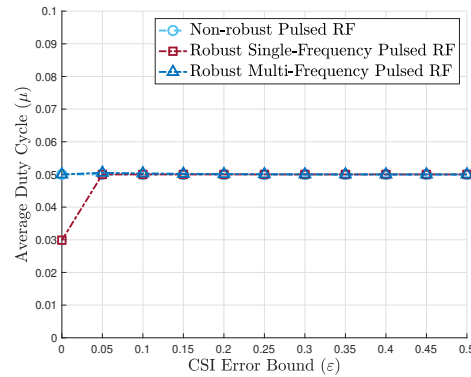


Fig. 3. Impact of channel uncertainty on duty-cycle selection.

over non-robust counterparts, while the MF approach yields up to $3\times$ performance gains. Future work will consider the development of schemes for setups with multi-diode rectifiers and impedance mismatch (both supported by the EH model), although the rectifier efficiency function used here corresponds to realistic non-ideal hardware with imperfect matching, and involve multi-antenna/multi-user extensions.

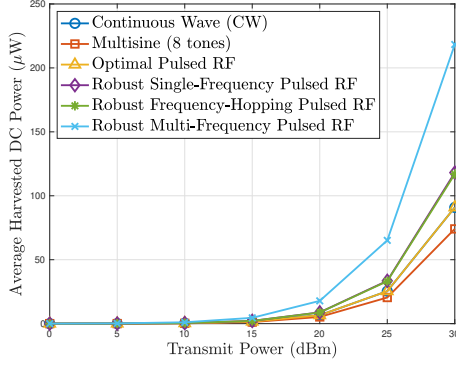


Fig. 4. Impact of transmit power on harvested power.

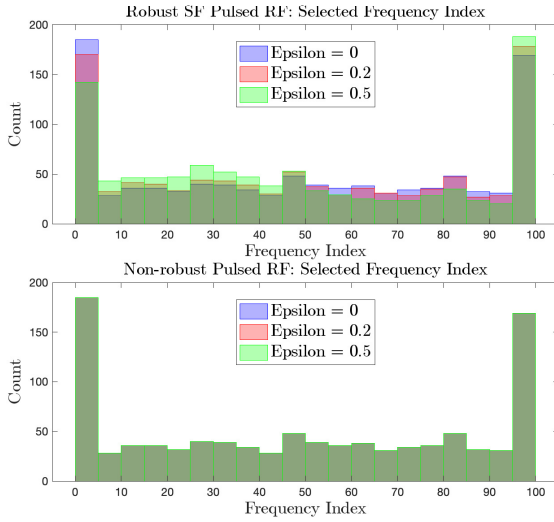


Fig. 5. Selection of frequencies for different CSI error levels.

APPENDIX A: COMPUTATION OF GRADIENTS

In the SCP algorithm, we have

$$\frac{\partial J}{\partial A_i} = \frac{\partial \mu^*}{\partial A_i} \cdot \eta(p_{\text{peak}}) \cdot p_{\text{peak}} + \mu^* \cdot \frac{\partial}{\partial A_i} [\eta(p_{\text{peak}}) \cdot p_{\text{peak}}], \quad (26)$$

where in the low-power regime,

$$\frac{\partial \mu^*}{\partial A_i} = \frac{2(1-\varepsilon)^2 A_i |\tilde{H}(f_i)|^2}{\bar{p}}. \quad (27)$$

Also,

$$\frac{\partial}{\partial A_i} [\eta(p_{\text{peak}}) \cdot p_{\text{peak}}] = [p_{\text{peak}} \cdot \eta'(p_{\text{peak}}) + \eta(p_{\text{peak}})] \cdot \frac{\partial p_{\text{peak}}}{\partial A_i}, \quad (28)$$

with

$$\begin{aligned} \frac{\partial p_{\text{peak}}}{\partial A_i} &= \frac{4(1-\varepsilon)^2 |\tilde{H}(f_i)| \sum_{k=1}^K A_k |\tilde{H}(f_k)|}{\mu^*} \\ &\quad - \frac{p_{\text{peak}}}{\mu^*} \cdot \frac{\partial \mu^*}{\partial A_i}. \end{aligned} \quad (29)$$

Likewise,

$$\frac{\partial^2 \mu^*}{\partial A_i \partial A_j} = \begin{cases} \frac{2(1-\varepsilon)^2 |\tilde{H}(f_i)|^2}{\bar{p}}, & \text{if } i = j \\ 0, & \text{if } i \neq j \end{cases}, \quad (30a)$$

$$\begin{aligned} \frac{\partial^2 p_{\text{peak}}}{\partial A_i \partial A_j} &= \frac{4(1-\varepsilon)^2 |\tilde{H}(f_i)| |\tilde{H}(f_j)|}{\mu^*} \\ &\quad - \frac{4(1-\varepsilon)^2 |\tilde{H}(f_i)| \sum_{k=1}^K A_k |\tilde{H}(f_k)|}{(\mu^*)^2} \left(\frac{\partial \mu^*}{\partial A_j} + \frac{\partial \mu^*}{\partial A_i} \right) \\ &\quad - \frac{\partial p_{\text{peak}}}{\partial A_i} \cdot \frac{1}{\mu^*} \cdot \frac{\partial \mu^*}{\partial A_j} - \frac{p_{\text{peak}}}{(\mu^*)^2} \cdot \frac{\partial \mu^*}{\partial A_i} \cdot \frac{\partial \mu^*}{\partial A_j} \\ &\quad - \frac{p_{\text{peak}}}{\mu^*} \cdot \frac{\partial^2 \mu^*}{\partial A_i \partial A_j}, \end{aligned} \quad (30b)$$

$$\begin{aligned} \frac{\partial^2}{\partial A_i \partial A_j} [\eta(p_{\text{peak}}) \cdot p_{\text{peak}}] &= \frac{\partial}{\partial A_j} [p_{\text{peak}} \cdot \eta'(p_{\text{peak}}) + \eta(p_{\text{peak}})] \\ &\quad \cdot \frac{\partial p_{\text{peak}}}{\partial A_i} + [p_{\text{peak}} \cdot \eta'(p_{\text{peak}}) + \eta(p_{\text{peak}})] \cdot \frac{\partial^2 p_{\text{peak}}}{\partial A_i \partial A_j}, \end{aligned} \quad (30c)$$

where

$$\begin{aligned} \frac{\partial}{\partial A_j} [p_{\text{peak}} \cdot \eta'(p_{\text{peak}}) + \eta(p_{\text{peak}})] &= \\ &= [2\eta'(p_{\text{peak}}) + p_{\text{peak}} \cdot \eta''(p_{\text{peak}})] \cdot \frac{\partial p_{\text{peak}}}{\partial A_j}. \end{aligned} \quad (31)$$

REFERENCES

- [1] I. B. F. de Almeida, L. L. Mendes, J. J. P. C. Rodrigues, and M. A. A. da Cruz, "5G waveforms for IoT applications," *IEEE Commun. Surv. & Tut.*, vol. 21, no. 3, pp. 2554–2567, third quarter 2019.
- [2] B. Clerckx *et al.*, "Fundamentals of wireless information and power transfer: From RF energy harvester models to signal and system designs," *IEEE J. on Sel. Areas in Commun.*, vol. 19, no. 12, pp. 4–33, January 2019.
- [3] B. Clerckx and E. Bayguzina, "Waveform design for wireless power transfer," *IEEE Trans. Signal Process.*, vol. 64, no. 23, pp. 6313–6328, December 2016.
- [4] S. Abeywickrama, R. Zhang, and C. Yuen, "Refined nonlinear rectenna modeling and optimal waveform design for multi-user multi-antenna wireless power transfer," *IEEE J. Sel. Topics Signal Process.*, vol. 15, no. 5, pp. 1198–1210, August 2021.
- [5] A. J. S. Boaventura and N. B. Carvalho, "Maximizing DC power in energy harvesting circuits using multisine excitation," in *IEEE MTT-S Int. Microw. Symp. Dig.*, June 2011, pp. 1–4.
- [6] Y. Huang and B. Clerckx, "Waveform design for wireless power transfer with limited feedback," *IEEE Trans. Wireless Commun.*, vol. 17, no. 1, pp. 415–429, January 2018.
- [7] M. R. V. Moghadam, Y. Zeng, and R. Zhang, "Waveform optimization for radio-frequency wireless power transfer: (invited paper)," in *Proc. IEEE 18th Int. Workshop Signal Process. Adv. Wireless Commun. (SPAWC)*, July 2017, pp. 1–6.
- [8] Z. Feng, B. Clerckx, and Y. Zhao, "Waveform and beamforming design for intelligent reflecting surface aided wireless power transfer: Single-user and multi-user solutions," *IEEE Trans. on Wireless Commun.*, vol. 21, no. 7, July 2022.
- [9] B. Clerckx and J. Kim, "On the beneficial roles of fading and transmit diversity in wireless power transfer with nonlinear energy harvesting," *IEEE Trans. Wireless Commun.*, vol. 17, no. 11, pp. 7731–7743, November 2018.
- [10] N. Ayir, T. Riihonen, and M. Heino, "Practical waveform-to-energy harvesting model and transmit waveform optimization for RF wireless power transfer systems," *IEEE Trans. Microw. Theory Techn.*, 2023.
- [11] M. Razaviyayn, M. Hong, and Z.-Q. Luo, "A unified convergence analysis of block successive minimization methods for nonsmooth optimization," *SIAM J. Optim.*, vol. 23, no. 2, pp. 1126–1153, 2013.